Recovery and Cleaning of Fine Hydrophobic Particles using the Reflux™ Flotation Cell

M.J. Cole[a*], J.E. Dickinson[a] and K.P. Galvin[a]
[a]Centre for Advanced Particle Processing and Transport,
Newcastle Institute for Energy and Resources,
The University of Newcastle, University Drive, Callaghan, NSW 2308, Australia

*Corresponding author email: M.Cole@uon.edu.au

Abstract

The Reflux Flotation Cell (RFC) consists of a vertical vessel located above a series of parallel inclined channels. This novel system, which is the inverse of an existing gravity separation system known as the Reflux Classifier, provides a powerful mechanism for enhancing bubble-liquid segregation. The usual link between the imposed gas flux and water recovery in the froth product is decoupled through this mechanism, resulting in the establishment of a concentrated bubbly zone throughout the upper section of the cell, and no froth zone. A downwards fluidization arrangement promotes strong washing of the flotation product, to remove the hydrophilic slimes from the hydrophobic concentrate. The mechanism also provides for strong control of the bias flux, allowing a significant positive bias flux to be established. A feed suspension of fine coal tailings containing hydrophobic coal and hydrophilic mineral matter was subjected to the novel flotation, providing an ideal basis for studying the interplay between the hydrophobic particle recovery, inferred by the combustible recovery, and the product grade, inferred by the mineral matter content of the product, expressed by the ash %. The feed ash % was about 43 weight %. The product cleaning was compared to firstly, the results from the tree flotation method, and secondly, a newer method known as Coal Grain Analysis (CGA). The RFC results were found to lie to the left of the tree curve, converging to the limit described by the CGA analysis. This work suggests the RFC and CGA provide a form of mutual validation on the limits of cleaning, though more work will be needed to confirm this finding. The RFC was operated with a volumetric feed flux of the order 1 cm/s, a rate comparable to that of conventional flotation systems, with the bias flux ranging from 0.0 cm/s to 1.9 cm/s. For a fixed gas flux of 1.1 cm/s, increases in the liquid bias flux from 0.0 cm/s to 1.0 cm/s resulted in a decrease in product ash from 18.2% to 7.8%, and a reduction in combustible recovery from the order 87% to 75.6%. Operating at the lowest gas flux of 0.6 cm/s, and the strongest bias flux of 1.9 cm/s yielded a low product ash of 6.7% at the reduced combustible recovery of 64%.

Keywords:

Desliming flotation, Fine particle flotation, Inclined channels, Reflux Flotation Cell, Fluidization.

1. Introduction

Froth flotation is a century-old beneficiation technique (Crabtree & Vincent, 1962) used in the coal and mineral processing industries to separate fine particles according to differences in surface hydrophobicity. In this way, hydrophobic particles are selectively attached to the bubbles, and separated from the hydrophilic particles via the gravitational rise of the bubbles relative to the liquid, resulting in an overflow stream rich in the (typically) valuable hydrophobic material, containing entrained hydrophilic particles, and an underflow stream high in hydrophilic particles. The entrainment of particles to the overflow is promoted by the upwards interstitial velocity of water through the froth phase relative to the vessel, which is higher than the nominal superficial velocity. The entrainment is therefore dominated by the relatively fine particles (generally termed slimes, <38 μm) due to their relatively low rates of sedimentation relative to the upwards interstitial fluid velocity. Formally, the flotation product consists of hydrophobic particles adhered to the air bubbles, while the entrained particles exhibit no such adhesion, usually due to their hydrophilic properties. Exceedingly fine hydrophobic particles, <20 μm, that fail to adhere due to their low inertia can also contribute to the entrainment. The hydrophilic particles, which usually dominate the entrainment, govern the contamination of the flotation product, reducing the concentrate grade. Further, the degree of entrainment is directly related to the upwards flux of water reporting to the overflow concentrate, which in turn is directly controlled by the imposed gas flux.

The purpose of this paper is to investigate the potential of a novel flotation system, the Reflux Flotation Cell, to achieve full recovery of the hydrophobic particles, and complete rejection of the hydrophilic particles, including the slimes that would otherwise entrain with the recovered water. Fine coal tailings offer an ideal and realistic flotation feed, containing a high percentage of naturally hydrophobic and hydrophilic components. The physical limits are assessed through application of the industry standard tree flotation method, and by a newer method known as Coal Gain Analysis (CGA).

In conventional froth flotation machines, such as mechanical and column cells, the separation performance achieved is inextricably linked with the ability to form two distinct and stable zones – a pulp zone and a froth zone. These two zones are separated by an interface and characterised by significantly different values in gas hold-up. Typically, the pulp (or collection) zone will have a gas hold-up less than 25%, abruptly rising to more than 60% at the pulp-froth interface, and further increasing as a function of froth height due to bubble coarsening and coalescence, where values can approach unity at the free surface (Yianatos et al., 1985; Yianatos et al., 1986; Finch et al., 2000). The necessity to preserve a clear discernment between the pulp and froth zones, and the desire to maintain a stationary position of the interface in the flotation vessel, constrains the imposed volumetric gas flux to the order of 1 cm/s (Yianatos & Henríquez, 2007). Moreover, this effectively limits the liquid feed flux to a similar value (Yianatos & Henríquez, 2007).

For successful particle extraction, a hydrophobic particle and gas bubble must collide, successfully adhere, and survive as an aggregate without particle detachment until collection. In mechanical cells, this collision between particles and bubbles is achieved by agitation in the pulp zone, whereas column cells typically utilise counter-current flow of the feed slurry and gas stream in the collection zone to initiate interception. In the Jameson cell, a high shear rate environment is generated within narrow downcomers when the feed slurry and gas stream are introduced, promoting the formation of fine bubbles and enhancing the process of particle-bubble collision and attachment. Furthermore, in the Jameson cell, secondary contacting of the particles and bubbles occurs in the tank pulp zone, prior to the bubbles disengaging from the pulp (Harbort et al., 2004). Irrespective of the particle-bubble collision mechanism, successful recovery requires these particle-laden bubbles to subsequently rise

through the vessel via their buoyancy, traverse the pulp-froth interface into the froth, survive conveyance in the vertical direction through the froth zone, and ultimately be collected as froth overflowing the cell launder.

Herein lies one of the inherent issues in conventional froth flotation – the reliance on froth stability for successful and effective separation performance, and thus the interplay between froth drainage and collapse. Neethling and Cilliers (2001) outline that the froth zone is of paramount importance to the separation performance achieved in a flotation cell, as the grade and recovery of the hydrophobic particles are intrinsically linked to the froth structure and stability. Bubble coalescence and rupture is a pervasive issue in the froth zone, resulting from the liquid drainage into the surrounding network of Plateau borders and nodes by a combination of gravity, capillary and viscous dissipation forces (Neethling & Cilliers, 2001). Further, as much as 80% of the gas flux can disengage at the free-surface of the froth (Neethling & Cilliers, 2001). Thus, bubble coalescence and rupture limits the mass pull of solids achieved (Hadler et al., 2010), and causes a loss in recovery as the detached particles drain back to the pulp zone. Further, the lack of both stability and permeability of flotation froths (Yianatos et al., 1987; Kruglyakov et al., 2010) can hinder the ability to effectively and uniformly apply wash water to the product to remove hydraulically entrained slimes.

While the limitations in ultrafine particle recovery by means of flotation are well known (Flint & Howarth, 1971; Trahar & Warren, 1976), recent technological developments have targeted improvements to ultrafine recovery via improved flotation hydrodynamics in order to minimise valuable materials loss to tailings. Flotation theory suggests that high shear rates in the air-slurry mixture and the formation of fine bubbles can enhance ultrafine particle recovery, improving the particle-bubble collision and attachment efficiencies, thus compensating for the low kinetic flotation rate of ultrafine particles (Jameson, 2009; Jameson, 2010). Three recent technologies focused on improving the recovery of ultrafine particles include the Concorde Cell (Jameson, 2010), the IMHOFLOT G-Cell (Imhof et al., 2007), and the StackCell™ (Mankosa et al., 2018). The Concorde Cell utilises a pressurised downcomer with a choke in order to achieve supersonic flow on exit of the downcomer and the subsequent formation of shock waves. The high shear zone results in the formation of very fine bubbles, and an impingement bowl located below the downcomer outlet results in both the formation of a vortex ring and redirection of the flow upwards in the separation vessel (Jameson, 2010). The IMHOFLOT G-Cell employs an external self-aerating unit prior to the downcomer, and feeds this aerated slurry tangentially into the separation vessel. The resulting centrifugal force enhances the froth separation, and hence lowers the cell residence time (Imhof et al., 2007; Wills & Finch, 2016). The StackCell™ also employs pre-aeration of the feed slurry, which then passes to a high-shear aerator for efficient particle-bubble collection (Mankosa et al., 2018). It is critical to emphasise that these new technologies continue to rely on a froth zone to upgrade the concentrate.

The Reflux Flotation Cell (RFC), presented below in Figure 1, is a novel flotation technology consisting of a vertical chamber located above a system of parallel inclined channels. The RFC uses a downcomer arrangement to promote particle-bubble collision and attachment (Dickinson et al., 2015), where compressed air is introduced to the feed slurry via a sparger tube. The inclined channels enhance bubble-liquid segregation within the system, an application of the Boycott effect (Boycott, 1920). This arrangement de-couples the inherent hydrodynamic relationship between the imposed gas flux and the liquid flux reporting to the overflow, thus enabling a controlled volume of liquid to report to the overflow. Further, the increased segregation between the liquid and gas phases enables operation well beyond the flooded state (Dickinson & Galvin, 2014), increasing the hydrodynamic window of operation. A plenum chamber located at the top of the cell applies downwards fluidization water,

producing an inverted fluidized bed. This arrangement is ideal for providing counter-current washing through a highly permeable and unified bubbly bed with a bubble volume fraction of order 0.5. While applying high levels of wash water to a conventional froth can cause bubble rupture and collapse due to a lack of froth resilience, the freely moving, more rigid spherical bubbles present in the concentrated bubbly bed of the RFC enables the effective rejection of entrained slimes, upgrading the product whilst preserving the integrity of the overflow.

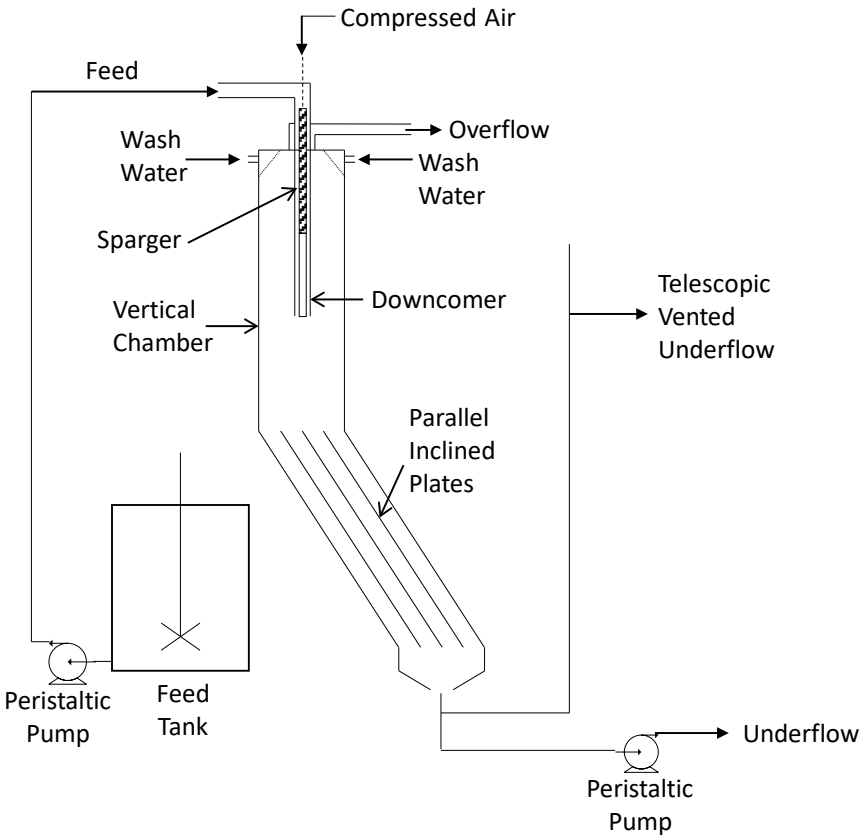

Figure 1: Schematic representation of the laboratory 20 L capacity Reflux Flotation Cell (RFC), depicting the experimental configuration. Important features of the RFC are outlined using unfilled arrow heads, while stream entry and exit locations are also illustrated, differentiated using filled arrow heads.

Previous investigations were concerned with two distinct modes of operation termed Fast Flotation and Desliming Flotation. Fast Flotation focused on increasing the feed flux, achieving up to a 10-fold increase over that of conventional flotation technologies (Dickinson et al., 2015). This single-stage rougher approach to flotation involves a short cell residence time, as low as 30 seconds (Dickinson et al., 2015), with little or no loss in recovery. Desliming Flotation focussed on achieving a high product grade at a high recovery. This was achieved by applying a downwards flux (termed positive liquid bias) of fluidization wash water through the top section of the cell, preventing hydrophilic entrainment to the product overflow (Dickinson & Galvin, 2014). The concentrated bubbly zone in the top section of the vertical column provides the ideal conditions for applying counter-current washing. The bubble volume fraction of ~0.5 provides strong permeability and hence flow of water (Lorenceau et al., 2009; Rouyer et al., 2010).

Initial investigations for processing high volumetric, low pulp density slurries, such as coal tailings, using the RFC involved the direct application of these distinct modes of operation in a two-stage rougher-cleaner flotation configuration. This approach was shown to produce robust separation performances, processing high volumetric throughput rates whilst achieving low ash coal products over two flotation stages (Jiang et al., 2016). However, a simpler approach to processing such streams may be realised by combining Fast Flotation and Desliming Flotation into a single flotation stage, which should offer substantial flowsheet and operational simplification, and cost reductions. Hence, analysing the interplay between recovery, product grade and throughput is critical for assessing the validity and applicability of the single stage approach. Examining the recovery-grade relationship of the single separation stage as a function of throughput is also of significant importance, and thus will be the subject of future work.

This paper commences this investigation by examining the recovery and cleaning of fine thermal coal sampled from a hydrocyclone overflow stream, using the RFC in a single stage of operation. In this study, the volumetric feed flux was set to a conventional level of about 1 cm/s to focus on the limits of cleaning and recovery.

A further goal of the present study was to compare the flotation performance achieved using the RFC with two established benchmarks for producing the grade-recovery curve. Feed samples were sent for external tree flotation analysis, in accordance with Australian Standard AS 4156.2.2, to determine the 'ideal' physical separation performance achievable. Feed samples was also analysed using a relatively new optical method, Coal Grain Analysis (CGA), to assess the maceral constitution and mineral abundance of every particle analysed in a given sample. Atkinson and Swanson (2018) have noted that CGA is analogous to SEM analysis of mineral samples. This study therefore provides a definitive assessment of the extent to which hydrophobic particle recovery can be maximized while also maximizing the rejection of hydrophilic slimes.

2. Experimental

2.1. Equipment and Feed Preparation

A laboratory scale Reflux Flotation Cell, schematically shown in Figure 1, was used in this study. The height of the cell was approximately 2 m, with both the vertical chamber of the cell, and the inclined section measuring approximately 1 m in length. The cross-sectional dimensions were 0.10 m × 0.080 m, hence the cross-sectional area was 0.008 m^2. This area was used in the calculation of all fluxes reported. The downcomer used to achieve contacting between the particles and the air bubbles consisted of a sintered steel sparger with a 10 µm media grade. The downcomer exit, 25.4 mm in diameter, was located half-way down the vertical chamber of the cell. Below the vertical chamber, the inclined section contained three 1 m long stainless steel plates, 1 mm in width. These plates produced four inclined channels of 19 mm perpendicular spacing, set at an angle of inclination of 70° with respect to the horizontal. Fluidization wash water, which entered the upper plenum chamber of the system, was distributed via a grid of 1.5 mm diameter holes. The product overflow from the RFC discharged the cell via a singular annular outlet located between the fluidization chamber and the downcomer.

The fine coal flotation feed used in this investigation was processed as-received from a hydrocyclone overflow sampled from a coal preparation plant situated in the Hunter Valley, Australia. No residual flotation reagents were present in the feed. For each experiment, the feed was prepared from a bulk supply, stored in 1.04 m^3 intermediate bulk containers (IBC). Two IBC's were agitated and pumped to

a 2 m^3 agitated tank for reagent conditioning. A small quantity of municipal water was used to transfer any solids remaining in the IBC. Prior to reagent addition, a feed sample was collected for tree flotation analysis and CGA. Diesel, used as a collector, was emulsified in a small quantity of municipal water prior to addition to the feed. After 10 minutes of conditioning time had elapsed, the frother, methyl-isobutyl-carbinol (MIBC), was added to the feed, and allowed to condition for a further 10 minutes. The concentrations of the reagents added were 3 kg/t solids and 20 ppm (volume basis), respectively. It is important to emphasise that no attempt was made to optimise the reagent dosage in this study. As this investigation was primarily a hydrodynamic study of the system, both the collector and frother dosages were selected to ensure reagent addition would not be a limiting factor, though significantly lower levels have been very effective in the past (Galvin & Dickinson, 2014; Galvin et al., 2014; Dickinson et al., 2015; Jiang et al., 2019). The fluidization wash water was prepared from municipal water, stored in 120 L drums, and dosed with equivalent frother concentration to the feed to ensure consistency in the bubble stability across the varying imposed fluidization water rates.

2.2. Feed Analysis

Three feed samples were processed by an external laboratory to generate the tree flotation data. Two tree flotation samples were collected from the conditioning tank prior to reagent addition, on different days, while the third sample was collected from the RFC feed tank after reagent addition had occurred. The tree flotation analysis, conducted in accordance with Australian Standard AS 4156.2.2 using diesel as collector, is a laboratory technique used to construct an 'ideal' or 'optimum' curve showing the cumulative recovery versus the cumulative weight % ash for a given feed (Pratten et al., 1989). The experimental technique consists of a series of batch flotation tests of a supplied feed in a mechanical cell, to determine the liberation-limited separation of the coal from the mineral matter. The procedure involves progressively re-floating the concentrate and tailings samples in order to fractionate the feed, without any recombination of samples, causing the methodology to branch out, comparable to the branches of a tree. Initial flotations are conducted at low collector dosages, or even in the complete absence of collector, in order to produce distinct data points in the low-ash (low recovery) portion of the curve. Further reagents are added at each step, particularly to the tailings samples, in order to maximise the potential recovery of coal (Mohanty et al., 1998). Historically the method has provided an important benchmark for flotation, though the procedure has attracted some conjecture concerning its representation as a benchmark, primarily due to issues arising from operator sensitivity and fine particle entrainment (Mohanty et al., 1998; Atkinson & Blanshard, 1999).

Three feed samples were also analysed by means of Coal Grain Analysis (CGA), a methodology used to determine the maceral constitution of every particle (>1 μm) set in a resin matrix. CGA is an optical imaging technique utilising the unique reflectance, texture and grain associations of maceral and mineral components in order to characterise each unique particle in the sample, also enabling the characterisation of the sample as whole. Via microscopic imaging, an estimation of the area of each maceral within a given particle, and the particle as an entirety, can be obtained. This information can then be utilised to estimate both the volume and the density of each particle, hence enabling the determination of their masses (Ofori et al., 2006; O'Brien et al., 2007). Previous work by O'Brien et al. (2013) has shown that the relative density of each maceral phase to be relatively constant, and hence the overall particle density can be simply computed as a function of the proportion of the maceral and mineral phases present. CGA groups the mineral phases into two categories, dark phase (low reflecting minerals) and bright phase (high reflecting) minerals, where the dark minerals are typically comprised of clays, carbonates and quartz, while the bright phases consist of minerals such as pyrite, iron oxides, and calcite (O'Brien et al., 2007; Hapugoda et al., 2010). Applying a relationship relating the mineral

phases present to an ash value allows the prediction of the ash content of each individual particle. Ordering the grains in terms of increasing ash content thus enables the construction of a recovery-ash curve. A more detailed description of the CGA technique is outlined in O'Brien et al. (2003) and O'Brien et al. (2007).

2.3. Continuous Flotation using the Reflux Flotation Cell

Prior to the start of each experiment, the conditioned feed was pumped as required in batches from the bulk conditioning tank to an agitated 0.5 m^3 intermediate holding tank, then continuously fed to a primary 0.15 m^3 agitated feed tank to maintain a fixed slurry level and constant feed rate to the RFC. Peristaltic pumps were used to pump the feed and fluidization wash water to the RFC. A peristaltic pump removed the bulk of the tailings flow. Further, a telescopic vented underflow was used to provide a further adjustment of the tailings flow rate, vented at approximately the same height as the downcomer outlet, to achieve an overflow liquid flux of 0.2 cm/s, and the desired liquid bias flux through the cell. A rotameter was used to set the gas flux entering the cell via the porous sparger.

The liquid bias flux, j_b, defined as the wash water flux entering the top of the flotation cell, less the overflow liquid flux exiting the top of the cell, provides a strong measure of the product cleaning achieved, and is visually represented in Figure 2. When the wash water flux is greater than the overflow liquid flux, there is a net downward flux of liquid, $j_b > 0$. Here, the bias is defined as positive. This is simply achieved by increasing the tailings rate by an order equal to the targeted liquid bias flux. When the wash water is less than the overflow liquid flux, there is net upward flux of liquid, $j_b < 0$. Here the bias flux is negative. If no wash water is applied, as is common in conventional rougher flotation operations, the bias flux is always negative provided there is overflow discharging from the cell. In the RFC, the top of cell is analogous to an inverted fluidized bed of spherical bubbles. The fluidization water functions as the wash water, and uniformly permeates downwards through the fluidized bed of high bubble volume fraction to reject the upward flux of hydrophilic particles. Thus, no froth zone exists in the RFC. Furthermore, the volumetric fractions of gas and liquid to the overflow are readily controlled through the independent control of the gas flux and liquid flux to overflow.

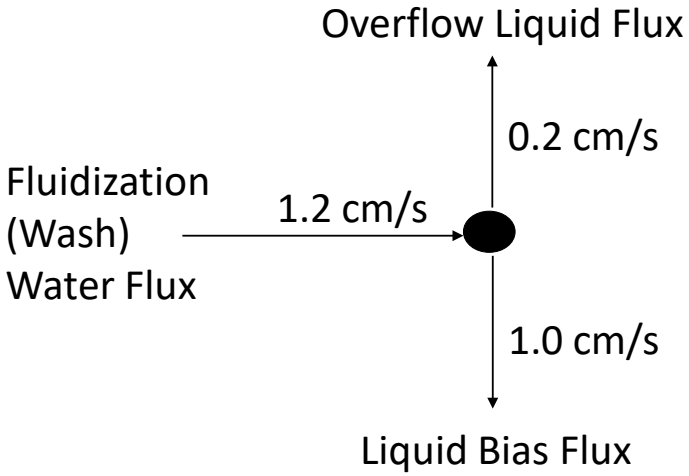

Figure 2: Representation of the liquid bias flux, defined as the fluidization (wash) water flux less the overflow liquid flux, with sample values taken from Run C.

For the experimental campaign, seven continuous, steady state experiments were conducted using a single-stage Reflux Flotation Cell. The liquid feed flux was held constant throughout the campaign at a value of 1.1 ± 0.1 cm/s, typical of the flux employed in conventional flotation circuits (Fuerstenau et al., 2007). As the flotation feed for each experiment was generated by randomly combining two IBCs of coal slurry, the feed pulp density across the series of runs varied slightly, ranging from 2.3 – 2.6 wt% solids. The liquid bias flux was increased from a value of 0.0 cm/s (neutral bias flux) in Run A, providing little desliming of the final product, to the extreme value of 1.9 cm/s in Run G, a value nearly double the feed flux entering the cell. Applying such an extreme downwards flux of liquid through a concentrated bubbly zone effectively inhibits slimes entrainment. In conventional flotation systems, these wash water flux values would result in froth rupture and collapse, and provide limited cleaning, at reduced recovery. The experimental operating parameters for the seven runs are outlined below in Table 1.

Table 1: Operating parameters for continuous steady state RFC runs A - G.

Run	Liquid Feed Flux (cm/s)	Feed Pulp Density (wt%)	Gas Flux (cm/s)	Fluidization Water Flux (cm/s)	Liquid Bias Flux (cm/s)	Gas Volume Fraction in the Overflow (-)
A	1.1	2.3	1.1	0.2	0.0	0.82
B	1.1	2.4	1.1	0.5	0.2	0.82
C	1.1	2.4	2.2	1.2	1.0	0.90
D	1.1	2.3	1.1	1.3	1.0	0.82
E	1.0	2.3	0.8	1.2	1.0	0.82
F	1.0	2.4	0.6	1.1	0.9	0.82
G	1.1	2.6	0.6	2.1	1.9	0.77

After several cell residence times of operation, multiple samples of the feed, product and reject were taken as a function of time. For each experiment, five head ash samples for each flow stream were collected in 1 L containers, sampled in the order of overflow, underflow and then feed. There was minimal lag time between collection of the three flow samples. The five repeat samples were obtained to confirm that steady state was reached, with each set of samples (overflow, underflow and feed) obtained sequentially with at least one cell residence time allowed between the next set of sampling. Timed samples of the overflow, underflow and feed streams were finally obtained in 20 L buckets. The overflow and underflow samples were taken simultaneously, quickly followed by the feed sample. The feed samples were collected from the feed tank, taking care to prevent any disturbances to the steady state operation of the cell.

The head ash samples were oven dried at 105°C and sent out to an external laboratory for ash analysis. Further, select timed samples were wet sieved at 38 µm and 20 µm, and dry sieved using the $\sqrt{2}$ sieve series prior to being sent out for external ash analysis. Due to the extremely small masses in the +20 µm sized fractions of the reject streams, some of the coarser size fractions were combined to obtain a sufficient mass for ash analysis. For the sake of consistency, the corresponding size fractions were also combined in the feed and product samples.

Mass balance reconciliation was applied to the mass rate, pulp density and head ash values and, where available, the particle size distribution and corresponding ash distribution data. An objective function

was formed using the sum of the squares of the adjustments, with a weighting factor applied to different measurement types. The square of the adjustment was divided by the square of the standard deviation. Here estimates of the standard deviation were used, set at 10% of the measured value. For the stream pulp density, which was averaged from five individual measurements, 5% of the measured value was used. For the head ash and fractional ash values, the highest precision of 1% of the measured value was used. The high precision on these ash values is a direct result of the accuracy of the ash analysis, reported with a repeatability of ±0.1% of the absolute ash value.

3. Results and Discussion

3.1. Feed Characterisation

Due to the fine nature of the particles comprising the hydrocyclone overflow feed stream, a Malvern Mastersizer 3000 was used to determine the feed particle size distribution. Figure 3 shows the feed cumulative volume percent of the particles as a function of the geometric mean particle size for five different feed samples, each collected over five separate continuous steady state experiments. The D_{50} of the feed was determined to have a mean value of 24.5 µm, with a 95% confidence interval of ±5.1 µm. Moreover, the average Sauter mean particle diameter, D_{32}, was determined to be 6.0 µm, with a 95% confidence interval of ±0.7 µm. The size distributions of the feeds were clearly consistent across the experiments.

Table 2 shows the particle size distribution determined using laboratory sieves, and the corresponding ash values, averaged from the results of Runs A, B, C and G. Further, Figure 4 shows the feed fractional ash percentage as a function of particle size for the four experiments (Runs A, B, C and G). As evident in both Table 2 and Figure 4, the majority of the hydrophilic gangue material is concentrated in the -20 µm size fraction, making up 91.2 % of the total mineral material feed mass. Similarly, 48.0 % of the combustible material was in this size fraction. This flotation feed would therefore be difficult to beneficiate and deslime, due to the large portion of ultrafines. Due to the fineness of particle size, the hydrophobic particles are difficult to recover, having a low kinetic constant, while the large portion of hydrophilic slimes is difficult to wash from the product.

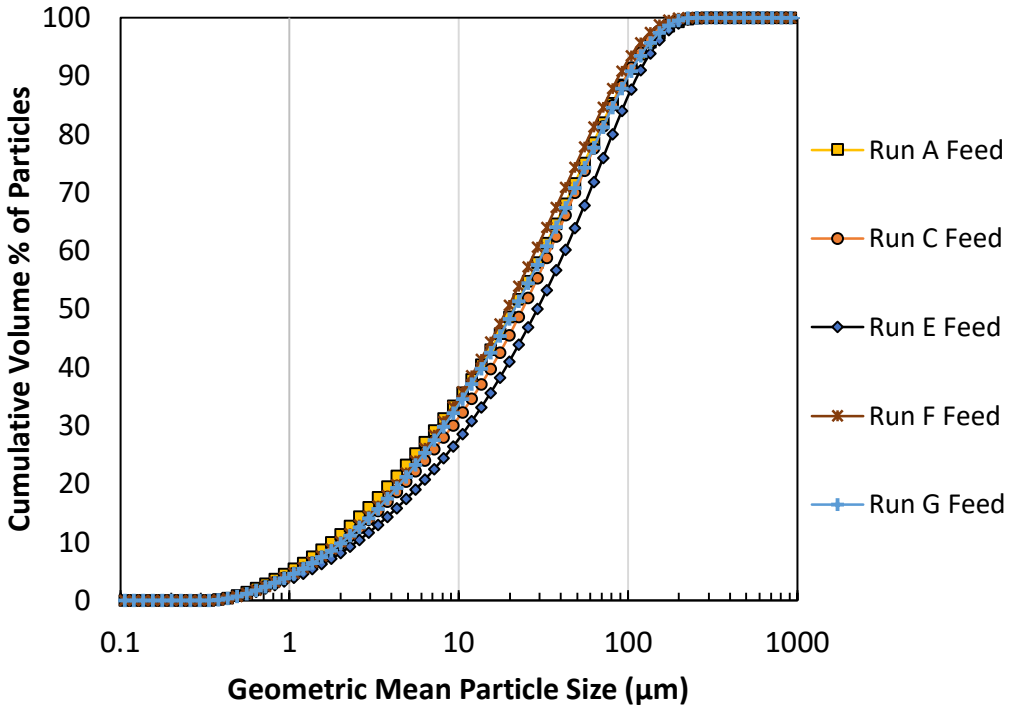

Figure 3: Flotation feed cumulative volume percent of particles as a function of geometric mean particle size.

Table 2: Particle size sieve distribution of the hydrocyclone overflow coal feed, and corresponding mass and ash fractions on a fractional and cumulative basis.

Particle size range (µm)	Fractional		Cumulative	
	Mass (%)	Ash (%)	Mass (%)	Ash (%)
-212 + 75	9.9	3.7	9.9	3.7
-75 + 38	13.1	8.3	23.0	6.2
-38 + 20	10.3	23.1	33.3	11.5
-20 + 0	66.7	59.2	100.0	43.3

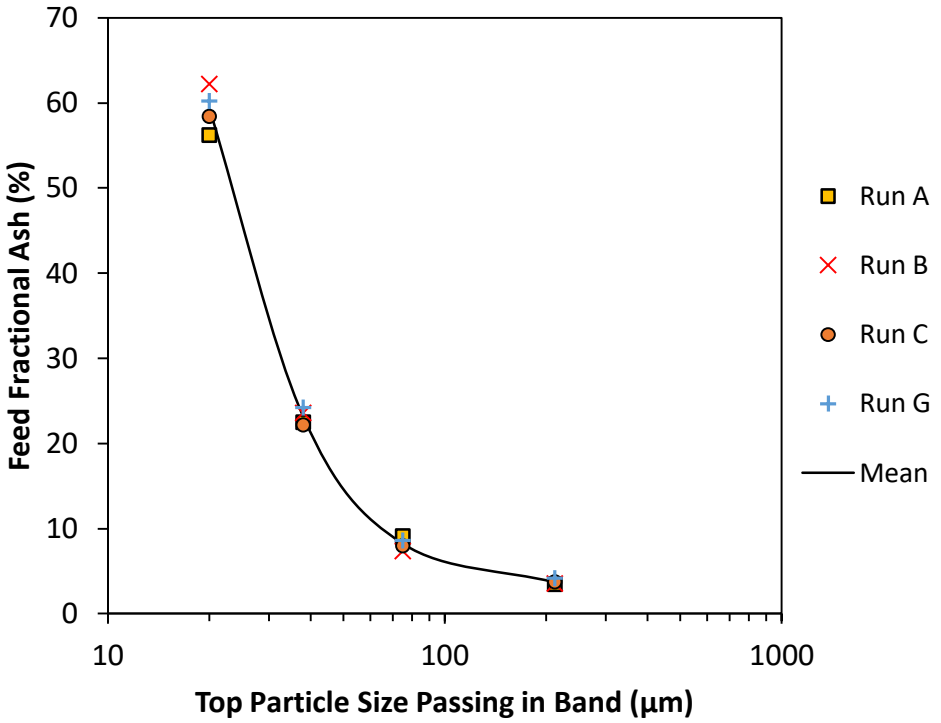

Figure 4: Feed fractional ash % as a function of particle size.

Three feed samples were processed by an external laboratory to generate the tree flotation data. Feed samples representative of the experimental campaign were also analysed using Coal Grain Analysis (CGA). Thus, the tree flotation methodology provided an experimentally derived recovery-ash curve generated from successive batch flotations, while the CGA result provided a feed characterisation based purely on the particles present in the feed sample, independent of any physical fractionation technique, in terms of the single, dominant and composite maceral components.

Figure 5 below shows the raw data for the predicted combustible recovery as a function of the product ash from each grain type identified in the feed using CGA. The data presented corresponds to a dosed feed sample, collected from the 0.15 m^3 feed tank supplying the RFC. The other two CGA samples provided similar maceral and mineral compositions. Of the 67.0% vitrinite detected, 58.3% and 35.8% were characterised as single component grains (>95% vitrinite) and dominant component grains (95% > vitrinite > 65%), respectively. 1.5% liptinite was detected, primarily deported in the vitrinite dominant and liptinite rich grain classes. 8.4% of the feed was characterised as inertinite, mostly present within composite grains. No bright mineral was reported across all grain classes. The remaining 23.1% was dark mineral scattered throughout the single, dominant and composite component grains, predominately within the minerite grain class, thus indicating high liberation of the mineral matter. The high maceral proportion of vitrinite as a single component grain is reflected by the steep gradient in the “All grains” recovery curve in Figure 5 over a narrow product ash range of 0 to 10 %.

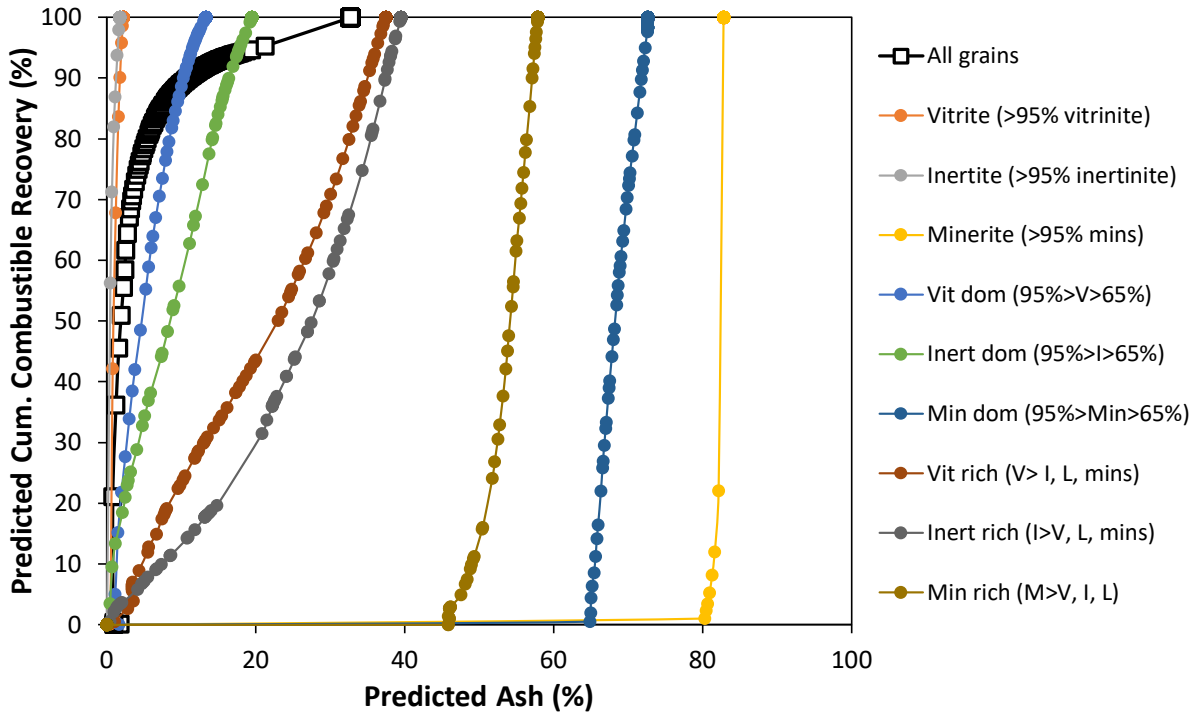

Figure 5: Raw Coal Grain Analysis results showing combustible recovery-ash curves.

It is important to note a slight correction was made to the CGA raw data to align the final head ash value of the feed with either the head ash values obtained from the tree flotation curves or the RFC experiments, depending on whether the sample was collected from the 2 m^3 conditioning tank prior to reagent addition or the 0.15 m^3 RFC feed tank after conditioning respectively. This correction was made on the assumption that the quantity of mineral matter required to align the head ash values had an ash percentage corresponding to that of the grain classification, pure minerite. A comparison of the CGA raw and corrected recovery-ash curves can be viewed in Appendix A. This adjustment likely reflects the composition of the very finest of particles, below 1 µm, neglected by the CGA method. Further, the specific feed presented issues in distinguishing the dark phase mineral matter (primarily clays) from the resin matrix used to mount the sample. Hence, the ash adjustment accounts not only for the <1 µm particles neglected by the method, but also the portion of mineral matter in the feed which was indistinguishable from the resin. This issue was considered feed specific, due to the mineral matter (clay) type present in the feed, and the fine nature of the particles reporting to the hydrocyclone overflow.

A comparison of the three tree flotation curves and the three recovery-ash curves generated from the corrected Coal Grain Analysis data is presented in Figure 6. The two tree flotation curves sampled prior to reagent addition show a high degree of consistency, evident from the comparable minimum ash values of order 7%, as well as the overall shape and trend of the data. These data contrast with the tree flotation curve generated from the sample collected after reagent addition, from the RFC feed tank. As is evident from the figure, the dosed tree flotation curve has been shifted to the right, and presents a compressed low-ash portion of the curve, culminating in a higher final feed ash. The compressed low-ash section of the curve is a result of the feed already being dosed with collector prior to the procedure, presenting great difficulty in fractionating the low ash coal. The tree flotation data also contrasts significantly with the CGA data shown in Figure 6. This suggests the physical fractionation achievable by the tree flotation methodology is relatively poor, despite being the

recognised benchmark for froth flotation. It is noteworthy that CGA, much like MLA for mineralogical analysis, utilises the two-dimensional area of a phase to determine the volume composition, and thus may over-estimate the extent of liberation of a given phase (Atkinson & Swanson, 2018). However, due to the large number of particles analysed in a given CGA sample, Atkinson and Swanson (2018) contend that this stereological error is of minor impact.

One noted discrepancy is the disparity of the final head ash value of the feed obtained from the tree flotation samples collected prior to reagent addition, at an approximate value of 35% ash, to that of the dosed tree flotation sample and the feed head ash samples obtained during the continuous steady state experiments, at an average value of 43% ash across the campaign. This was likely the result of the equilibrium condition established when pumping the conditioned feed slurry between three agitated tanks, resulting in a layer of froth forming on each tank. This froth, primarily composed of coal particles, should result in a net increase in the mineral matter content of the feed. The relatively low solids pulp density of the feed (~2.4 wt%) indicates that the feed ash % is particularly susceptible to this effect. Further, the final head ash of the tree flotation curve generated from the feed sample collected from the 0.15 m^3 RFC feed tank, after reagent dosing, confirms the reduction in coal and increase in mineral matter. Nonetheless, the five feed head ash samples collected from the feed tank confirm the feed ash to be consistent over each experiment. It is also noted that the head ash of the tree curve is a weighted summation of numerous flotation products, so carries additional error.

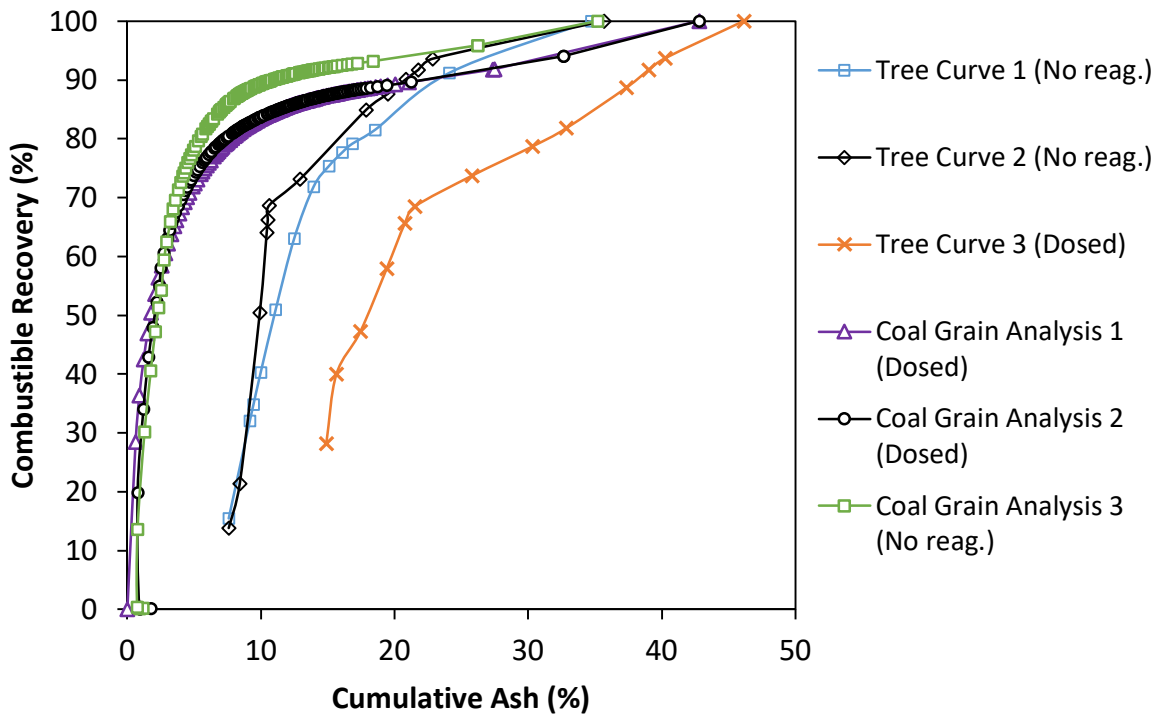

Figure 6: Comparison of the recovery-ash curves generated by the tree flotation methodology and the Coal Grain Analysis procedure, for feed samples collected prior to and after reagent addition.

3.2. Continuous Reflux Flotation Cell Results

Given the available feed, each continuous, steady state experiment was run for as long as possible to ensure the steady state condition was achieved, supported by the collection of five steady state head ash samples of each flow stream (feed, overflow and underflow), sampled at four minute intervals. Figure 7 shows as an example, the five raw head ash samples of the feed, overflow and underflow collected sequentially with time during Run F. The run time was referenced to the moment that overflow first discharged from the cell. As depicted in Figure 7, the ash percent for each of the three flow streams was consistent over a 16 minute interval, equivalent to almost twelve cell retention times. Other runs involved sampling periods of up to 20 cell retention times, with a minimum of 10. These data sets demonstrate steady state, moreover, the reliability of the combustible recovery and product ash value recorded for a given experiment. Further, the head ashes for the other six experiments displayed the same consistency with time, as shown in Appendix A.

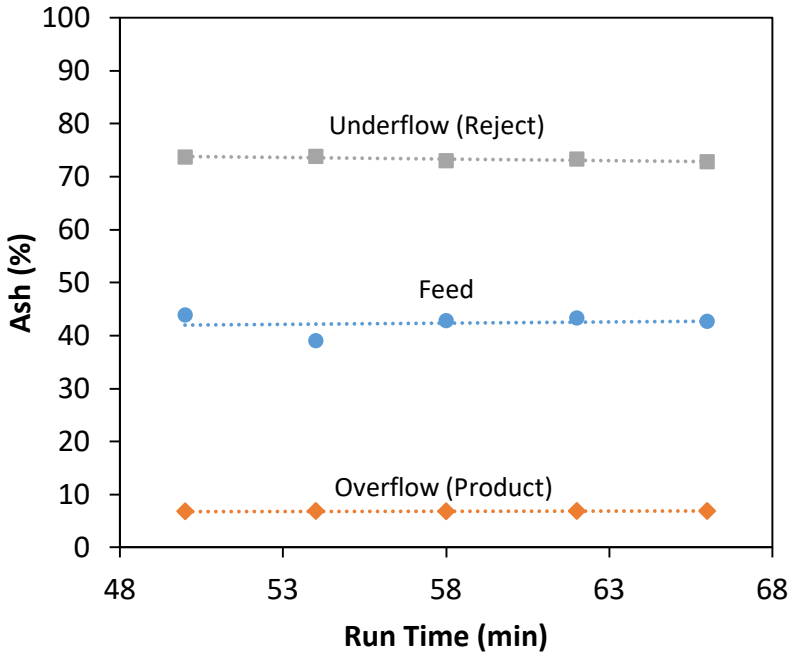

Figure 7: Raw feed, overflow and underflow head ash samples collected for Run F, plotted as a function of experiment run time. The consistency of ash percentage in each stream as a function of time indicates that steady state was successfully achieved.

A summary of the separation performance achieved for each of the seven experiments is given in Table 3. The mass yield and combustible recovery for each run was calculated using the two-product formula on an ash assay basis from the mass balance reconciled data. Again, due to the random selection and combination of IBC's to produce the flotation feed from bulk supply of hydrocyclone overflow, the feed ash value for each experiment exhibited slight variation, with a minimum value of 40.3% obtained in Run C, to a maximum of 44.9% in Run A. Nevertheless, the feed ash values were consistent throughout the campaign, at an average value of 42.8% ash.

Table 3: Summary of the separation performance data achieved using the RFC for runs A – G.

Run	Product Pulp Density (wt%)	Reject Pulp Density (wt%)	Feed Ash (%)	Product Ash (%)	Reject Ash (%)	Mass Yield (%)	Combustible Recovery (%)
A	5.6	1.0	44.9	18.2	82.0	58.1	86.3
B	6.0	0.9	44.0	12.1	84.4	55.9	87.7
C	5.1	0.6	40.3	6.7	75.3	51.0	79.7
D	4.6	0.6	42.2	7.8	73.1	47.4	75.6
E	6.2	0.6	42.2	7.7	73.8	47.8	76.4
F	8.6	0.7	42.5	6.9	72.9	46.0	74.6
G	6.3	0.6	43.8	6.7	67.1	38.5	64.0

Figure 8 shows the combustible recovery for Runs A – G, plotted as a function of the product ash achieved. Again, it is important to emphasise that whilst the result for each experiment is reduced to a single point reflecting the product ash and combustible recovery, the values plotted have been averaged from five sequential steady state samples, providing a high degree of confidence around each result. A comparison to the averaged tree flotation curves sampled prior to reagent addition, and the averaged "All grains" recovery-ash curve generated from the corrected CGA data from the dosed feed samples is included in Figure 8. The average tree flotation curve for the feed samples collected prior to reagent addition was included in lieu of the curve obtained from the dosed feed, as the result better indicates the low-ash portion of the curve, which is of most significance for comparison to the RFC results. The CGA recovery-ash curve however was averaged from the two dosed feed samples, as these samples were most representative of the feed processed in the continuous experiments as they were collected from the tank directly feeding the RFC. As the CGA is an optical imaging technique, the dosed feed should not have any deleterious effect on the generated recovery-ash result.

Typical separation performance achieved by industrial mechanical flotation cells often lie below and to the right of the knee of the tree flotation curve (Galvin et al., 2014). The RFC data set appear to the left of the tree flotation curve and appear to converge close to the CGA curve indicating the RFC achieved almost perfect cleaning. In fact, Run B and C appear to exceed the limit of the CGA recovery-ash curve. These should be deemed equivalent however due to the presence of data uncertainty.

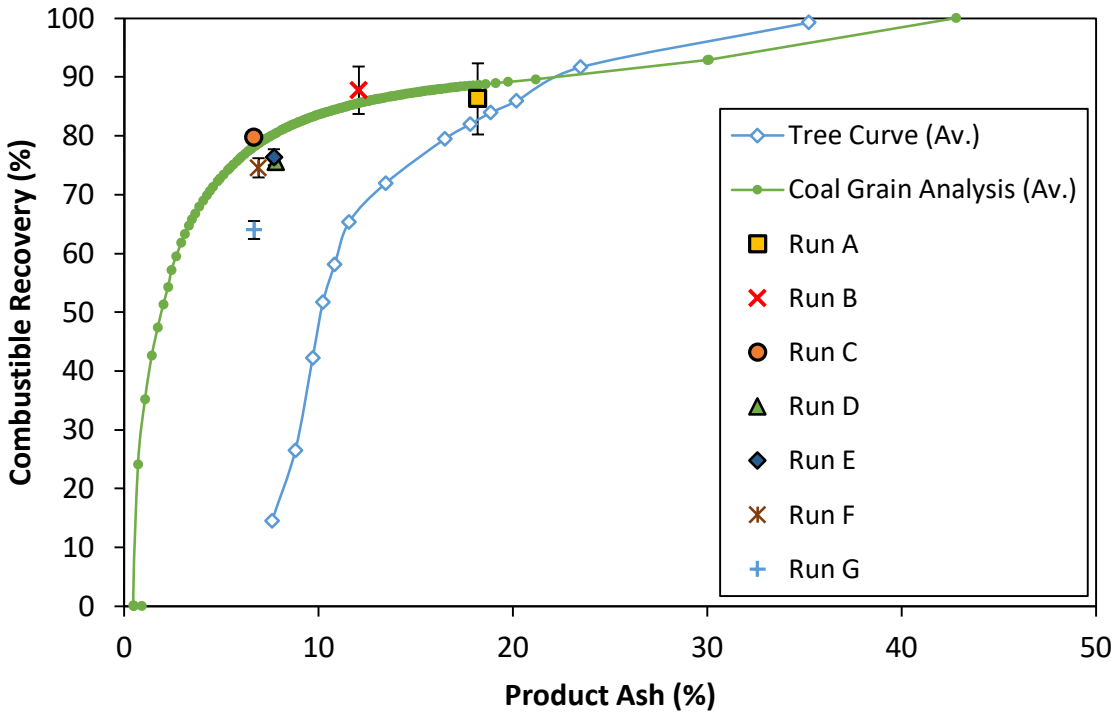

Figure 8: Combustible recovery (%) for Runs A - G as a function of product ash (%). The average of the two tree flotation curves sampled prior to reagent addition is also depicted, along with the averaged recovery-ash curve for the two dosed feed samples, generated from the Coal Grain Analysis (CGA).

Run A was completed with a neutral liquid bias flux (j_b = 0.0 cm/s), where the applied fluidization water flux was equal to the liquid overflow flux. As illustrated in Figure 8, the result agrees well with the tree flotation curve, and lies minimally below the CGA recovery-ash curve, achieving a combustible recovery of 86.3% at 18.2% product ash. This result is very respectable, achieved with a minimal cleaning effort. In an ideal scenario, the application of a neutral liquid bias flux should effectively neutralise the potential for fine particles to be hydraulically entrained to the overflow product. However, the no-slip boundary condition at the bubble surface ensures some upwards entrainment with the bubbles with some downwards liquid flow between adjacent bubbles, combining to produce the neutral bias flux. Thus strong positive bias is needed to minimise the upwards entrainment.

In Run B, the modest positive bias flux of 0.2 cm/s resulted in a 6.1% reduction in product ash to 12.1%. Moreover, this reduction in product ash was achieved whilst obtaining a slight increase in combustible recovery to 87.7%, significantly outperforming the tree flotation curve for the corresponding product ash %. As is evident from Figure 8, the result for Run B also lies slightly above the recovery-ash curve generated from the CGA data, emphasising the separation performance of the RFC and the significance of the result. The result should be considered equivalent to the limit defined by the CGA curve, due to the presence of data uncertainty.

In Run C, the liquid bias flux was increased significantly to 1.0 cm/s and the gas flux to 2.2 cm/s, resulting in a much lower product ash of 6.7%, while combustible recovery remained very high at 79.7%. Interestingly, the very lowest ash % obtained in the tree flotation tests was 7.6%, at a corresponding combustible recovery of 14.5%. More significantly, this result also matches the limit of

the CGA. However, the Run C feed ash was lowest amongst all the runs, which may account for the recovery lying higher than the high precision of results for Runs D-F obtained also using a 1 cm/s bias flux. Based on these results it is concluded that the CGA result describes the true limit of the flotation separation provided the CGA sample is a true representation of the flotation feed. More work is needed to confirm this finding.

Runs D – F were completed by maintaining a positive liquid bias flux of order 1 cm/s while also reducing the gas flux. By reducing the applied gas flux, while maintaining the imposed positive liquid bias flux, a greater cleaning efficiency should in principle be realised. However, the reduction in the gas flux yielded no further benefit, suggesting in this case the strong downwards flux of liquid, alone, was sufficient. It is anticipated, however, that at a lower bias flux there would be some benefit to the cleaning from a reduction in the gas flux.

The effects of an extreme liquid bias flux of 1.9 cm/s was investigated in Run G, at a modest gas flux of 0.6 cm/s. Similar to Runs C – F, the product ash remained consistent at 6.7%, however a significant reduction in combustible recovery was observed, dropping from the order of 75% in Runs D – F to 64.0% in Run G. Certainly, the extreme positive liquid bias flux provided by the fluidization wash water would impart a significant shearing force on the surface of the bubbles as the liquid travels downwards, flowing over the bubble surface and through the interstitial liquid separating them. Further, Runs F and G were conducted at the same feed flux of 1.0 ± 0.1 cm/s and gas flux of 0.6 cm/s, presenting virtually identical conditions in the downcomer for particle collision and attachment. Thus, the decrease in recovery from Run F to Run G was arguably due to the selective stripping of less hydrophobic particles from the surface of the bubble. This phenomenon has previously been reported by Galvin and Dickinson (2014) and Galvin et al. (2014). Of course, it is improbable that such a bias flux would be employed in the industry.

These results demonstrate the effectiveness of using inverted fluidization through a bubbly bed to reject slimes, enabling a low ash coal product to be obtained at a high combustible recovery, all in a single flotation stage. The significant permeability offered by a concentrated bubbly zone with a bubble volume fraction of order 0.5 (Lorenceau et al., 2009; Rouyer et al., 2010) enables the applied fluidization wash water to uniformly and effectively reject slimes when a downwards (positive liquid bias) flux of liquid is applied. This contrasts conventional flotation, which relies on a natural upgrading process via the drainage of the entrained liquid and associated slimes through a network of plateau borders and nodes within the structure of the froth. Here, the thinning liquid lamella between the bubbles in the froth zone limits the permeability and hence the potential for froth washing, while also causing the bubbles to coalesce and rupture, and in turn release hydrophobic product.

The mass yield decreased as the liquid bias flux increased. A mass yield of 58.1% was achieved in Run A, where a neutral liquid bias of 0.0 cm/s was employed, and decreased to 55.9% in Run B, at a corresponding bias flux of 0.2 cm/s. Increasing the liquid bias flux to 1.0 cm/s resulted in a further decrease in the mass yield, to 51.0%. The mass yield was then consistent at 47% as the bias flux was maintained. The observed decrease in mass yield up to this point, from 58.1% in Run A to 46.0% in Run F, is primarily due to the reduced hydraulic entrainment of ultrafine gangue material, namely the minerite bearing grains, given the decreasing product ash %. A further increase in the bias flux to an extreme level of 1.9 cm/s reduced the mass yield to 38.5%. A comparison of the raw and mass balanced yields determined via solids flow rates and by means of ash assay is located in Appendix A. This trend is similar for the combustible recovery across the experimental range, however, the reduction in recovery is lower. The highest combustible recovery of 87.7% was achieved in Run B where a liquid bias flux of 0.2 cm/s was employed, however, within the limits of uncertainty, both

Runs A and B achieved essentially the same recoveries. The minimum combustible recovery of 64.0% was achieved in Run G, where the extreme liquid bias flux of 1.9 cm/s was used.

Figure 9 and Figure 10 show the effect of the liquid bias flux on the combustible recovery and product ash % respectively for the seven experiments. Clearly, there is strong correlation with the liquid bias flux. The results also indicate that the initial increase in the liquid bias flux results in significant improvements in product desliming, however beyond a bias flux of 1 cm/s, no further benefit to the product grade (ash %) is observed.

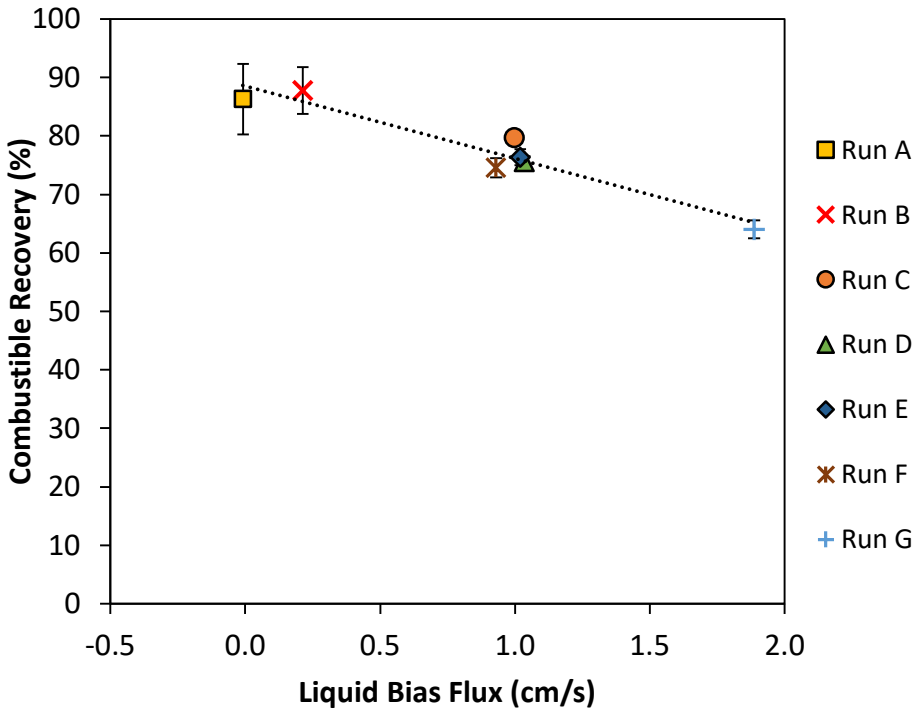

Figure 9: Combustible recovery for Runs A - G as a function of liquid bias flux. Error bars indicate 95% confidence intervals, however for some results are obscured by the symbol.

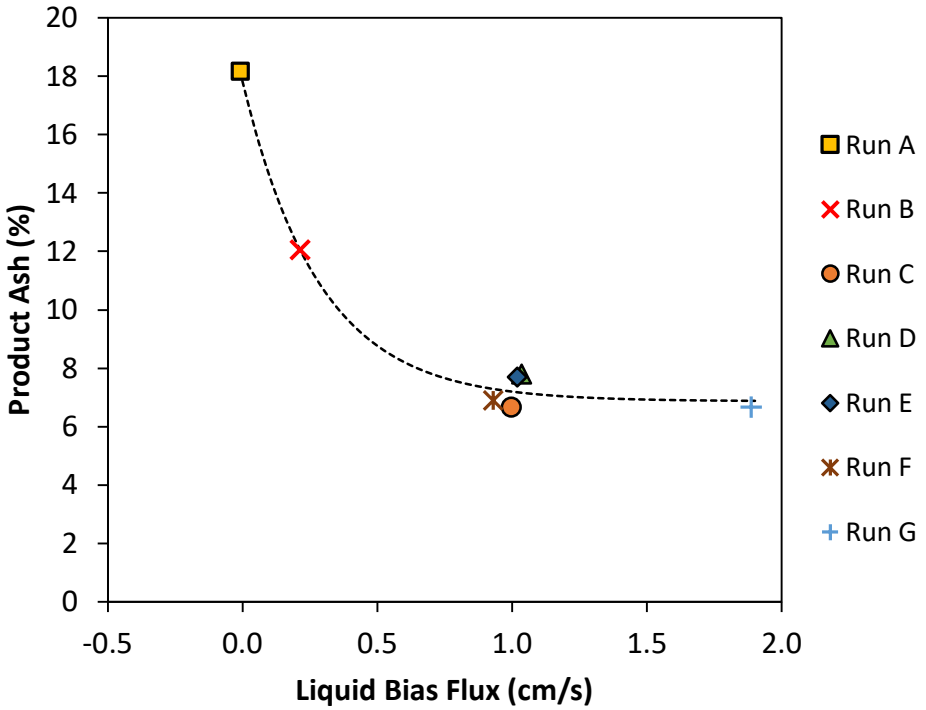

Figure 10: Product ash for Runs A - G as a function of liquid bias flux.

Table 4 shows the fractional and cumulative mass and ash fractions for the flotation feed, product and reject streams for Run C. Further, Table 5 presents a closer examination of the separation performance by size for Run C. Figure 11 shows the fractional combustible recovery for Runs A, B, C and G as a function of particle size. The combustible recovery tends to be highest for the coarser sized particles, decreasing as the particles size decreases. For Runs A-C, the combustible recoveries were very high over the +20 µm size range. In fact, for Run C, covering the +20 µm portion the cumulative recovery was 90.9% and cumulative ash 5.2%. As expected, complete recovery of the finest particles proved most difficult, where a maximum fractional recovery of 79.5% of the -20 µm particles was achieved in Run A, using a neutral liquid bias flux.

From Figure 11 it is also clear that fractional recovery by particle size was consistent for Runs A and B, within error, with both experiments operated using modest fluidization fluxes and liquid bias fluxes. By increasing the liquid bias flux to 1.0 cm/s in Run C, a relatively uniform decrease in fractional recovery for each particle fractional size was revealed. This trend was further evident when examining the results achieved using the extreme positive liquid bias flux of 1.9 cm/s in Run G. This suggests that the decrease in recovery was due to a dominant stripping effect, imparting a large shearing force on the bubble surface and ultimately inducing a degree of particle detachment relative to the downwards fluid flux. Bubble coalescence may also have been induced.

Figure 12 shows the product ash % as a function of particle size for Runs A, B, C and G. Clearly, by increasing the liquid bias flux, a significant reduction in the product ash of the -38 µm, and especially the -20 µm material is observed. The fractional product ash of the -20 µm material was seen to decrease from 25.2% in Run A down to a minimum of 9.3% in both Runs C and G. This further emphasises the effectiveness of using an inverted fluidized bed of clean water to reject fine slimes.

Table 4: Fractional and cumulative mass % and ash % by size fractions for the flotation feed, product and reject for Run C.

Particle size range (µm)	Flotation Feed				Flotation Product				Flotation Reject			
	Fractional		Cumulative		Fractional		Cumulative		Fractional		Cumulative	
	Mass (%)	Ash (%)	Mass (%)	Ash (%)	Mass (%)	Ash (%)	Mass (%)	Ash (%)	Mass (%)	Ash (%)	Mass (%)	Ash (%)
-212 + 75	11.6	3.7	11.6	3.7	21.6	3.2	21.6	3.2	1.2	14.1	1.2	14.1
-75 + 38	15.6	8.0	27.2	6.2	26.8	5.2	48.4	4.3	3.8	28.2	5.0	24.8
-38 + 20	10.7	22.2	37.9	10.7	15.2	8.0	63.7	5.2	6.1	59.3	11.1	43.6
-20 + 0	62.1	58.4	100.0	40.3	36.3	9.3	100.0	6.7	88.9	79.3	100.0	75.3

Table 5: Separation performance by size for Run C.

Particle size range (µm)	Fractional Yield (%)	Fractional Recovery (%)
-212 + 75	94.9	95.5
-75 + 38	87.9	90.6
-38 + 20	72.3	85.5
-20 + 0	29.8	65.0

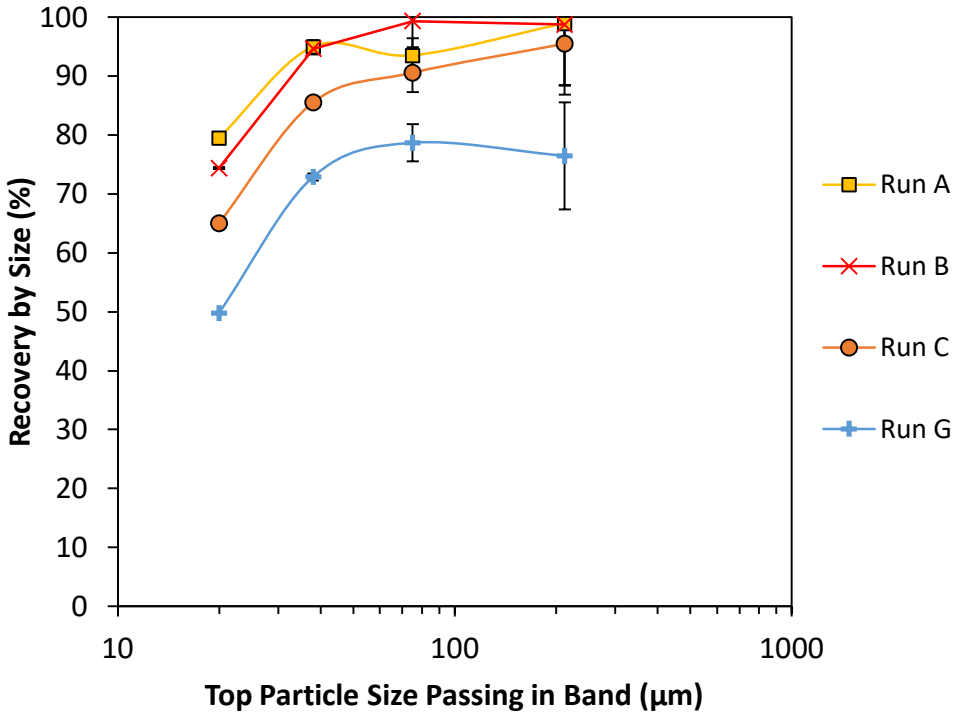

Figure 11: Fractional combustible recovery by particle size for Runs A, B, C and G. Error bars represent ±95% confidence intervals.

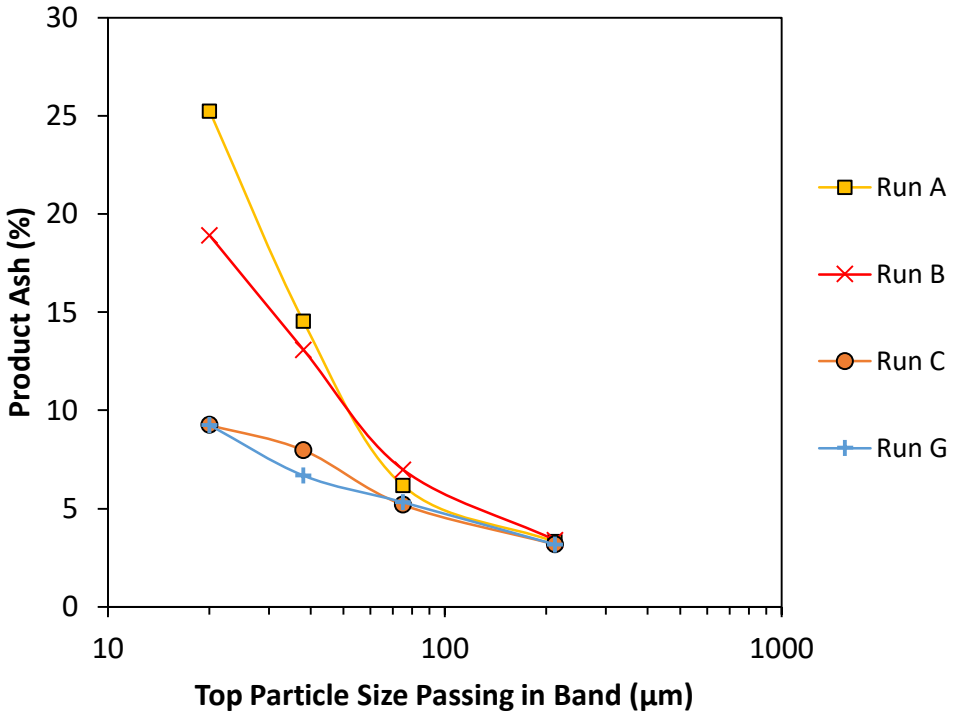

Figure 12: Fractional product ash (%) by particle size for Runs A, B, C and G.

Schulz (1970) proposed an approach for quantifying the technical separation efficiency, *E*, based on the recovery of both the valuable and non-valuable material in a given product. For the separation efficiency of a coal sample, Jiang et al. (2016) determined $E = R_c - (100 - A)$, where R_c is the combustible recovery, and *A* the ash rejection, defined as the ash present in the feed that reports to the reject stream. Thus the ash rejection *A* can be determined by $(100 - R_g)$, where R_g is the recovery of gangue in the product stream. It is important to emphasise that the separation efficiency is a measure of the separation performance achieved for a given feed and does not reflect any economic considerations (Wills & Finch, 2016). Indeed, separations that occur very close to the CGA curve, corresponding to the true physical limit of cleaning for a given feed, can be considered to be 100% efficient even though the value of *E* is clearly lower.

Figure 13 shows the separation efficiencies for the seven RFC experiments, given by the combustible recovery as a function of the ash rejection *A*. The perpendicular, dashed, lines shown in the figure represent the spectrum of separations possible for a given separation efficiency. As is evident from the figure, by progressing to the very top-right corner of the plot, a perfect separation efficiency of 100% is realised, describing complete recovery of a fully liberated feed with perfect selectivity for the valuable material. Also presented in Figure 13 is the 'ideal' separation efficiency curve generated from the CGA data. The CGA curve shows the maximum achievable for this feed is $E = 71.5\%$, reflecting the presence of mineral matter within the coal macerals. The recovery and product ash values corresponding to the maximum are 81.9% and 8.6%, respectively, suggesting from Figures 9 and 10 a liquid bias flux near 0.6 cm/s would deliver the best separation for this feed.

The continuous steady state RFC experiments show excellent separation efficiencies with some results marginally better than the technical separation efficiency given by the CGA results. These should be deemed to be equivalent given the existence of data uncertainty, and of course, the slight discrepancy

in the CGA sample and RFC feed sample discussed previously. Run C achieved a separation efficiency, *E*, of 71.3% at a combustible recovery of 79.7%. The greatest separation efficiency achieved was 72.4% in Run B, where a slight decrease in ash rejection compared to Run C was compensated by a higher combustible recovery.

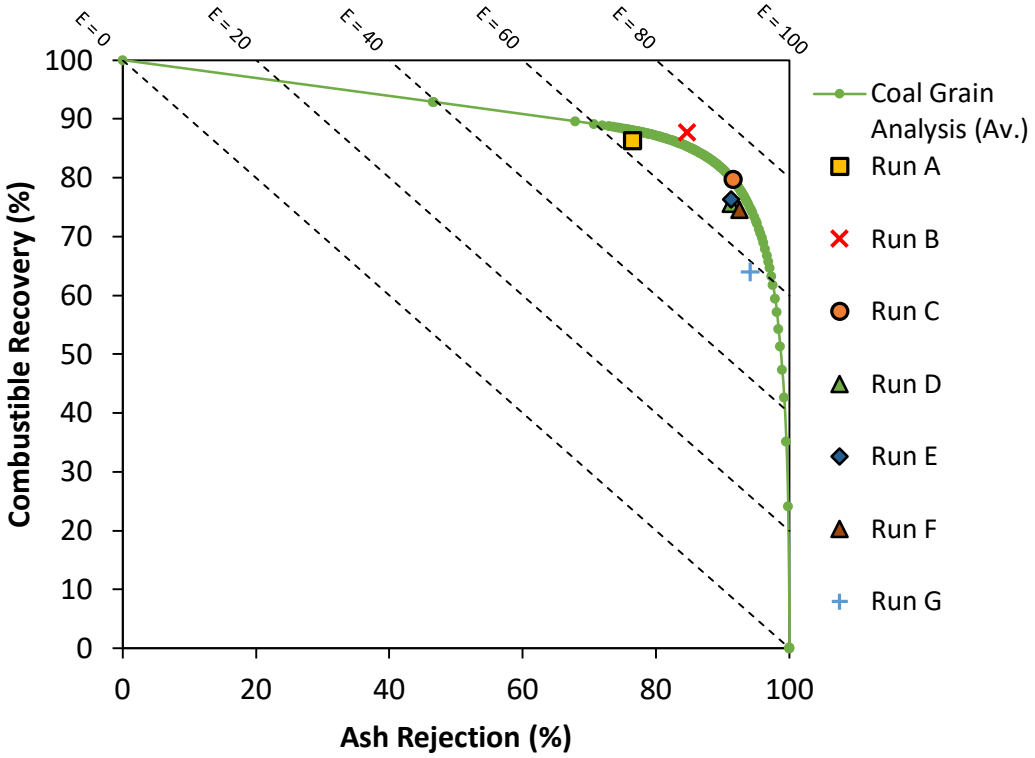

Figure 13: Separation efficiency for Runs A – G, plotting the ash rejection, which represents the ash in the feed that reports to the reject stream, as a function of combustible recovery. Also presented is the ideal separation efficiency curve for the specific coal feed using a single flotation stage, generated using the CGA data.

4. Conclusions

In this study, the interplay between hydrophobic particle recovery and hydrophilic particle rejection, inferred by the combustible recovery and product grade was investigated using the Reflux Flotation Cell (RFC). The flotation feed, which consisted of a well-liberated coal slurry feed normally discarded to tailings, was introduced at a volumetric flux of order 1 cm/s, with the liquid bias fluxes ranging from 0.0 cm/s to 1.9 cm/s. The results demonstrated that an increase in the liquid bias flux, from a neutral liquid bias flux in Run A to a positive liquid bias flux of 0.2 cm/s in Run B, resulted in a significant decrease in product ash from 18.2% to 12.1% ash. The product ash decreased to 6.7% ash in Run C at a bias flux of 1.0 cm/s. Thus, increases to the liquid bias flux resulted in reduced entrainment, and hence the attainment of lower ash products, until the product ash was constrained by the liberation-limited characteristics of the feed. Combustible recoveries in the range 75 – 88% were achieved, diminishing further at an extreme liquid bias flux of 1.9 cm/s where selective stripping was induced on the basis of particle surface hydrophobicity. An inverse relationship was clearly evident between the imposed liquid bias flux and the combustible recovery. Importantly, when applying a downwards flux of fluidization water, the results lay well to the left of the tree flotation curve. The consistently

superior RFC results highlight issues with the tree flotation methodology in describing the ideal separation performance achievable by flotation. Significantly, the results converged towards the theoretical limit defined by the Coal Grain Analysis curve.

5. Acknowledgements

The authors acknowledge the financial support of ACARP and FLSmidth for our on-going collaboration in developing the Reflux Flotation Cell technology. The University of Newcastle has an R&D Agreement with FLSmidth, and an IP policy that extends benefits to inventors.

6. References

Atkinson, B., & Blanshard, S. (1999). Improved Measure of Ultimate Flotation Performance, ACARP Project C6044 Final Report, Australian Coal Association.

Atkinson, B., & Swanson, A. (2018). Adaptation of Coal Grain Analysis to Improve Flotation Yield Estimation, ACARP Project C24045 Final Report, Australian Coal Association.

Boycott, A.E. (1920). Sedimentation of blood corpuscles, *Nature*, *104:152*, 532.

Crabtree, E.H., & Vincent, J.D. (1962). Historical outline of major flotation developments. In Fuerstenau D.W*., Froth flotation: 50th anniversary volume* (pp. 39-54). New York: The American Institute of Mining, Metallurgical and Petroleum Engineers.

Dickinson, J.E., & Galvin, K.P. (2014). Fluidized bed desliming in fine particle flotation – Part I, *Chemical Engineering Science*, *108*, 283-298.

Dickinson, J., Jiang, K., & Galvin, K. (2015). Fast flotation of coal at low pulp density using the Reflux Flotation Cell, *Chemical Engineering Research and Design*, *101*, 74-81.

Finch, J.A., Xiao, J., Hardie, C., & Gomez, C.O. (2000). Gas dispersion properties: bubble surface area flux and gas holdup, *Minerals Engineering*, *13*, 365–372.

Flint, L.R., & Howarth, W.J. (1971). Collision efficiency of small particles with spherical air bubbles, *Chemical Engineering Science*, *26*, 1155.

Fuerstenau, M.C., Yoon, R.H., & Jameson, G.J. (Eds.). (2007). *Froth flotation: A century of innovation*. Littleton, CO: Society for Mining, Metallurgy, and Exploration.

Galvin, K.P., & Dickinson, J.E. (2014). Fluidized bed desliming in fine particle flotation – Part II flotation of a model feed, *Chemical Engineering Science*, *108*, 299–309.

Galvin, K.P., Harvey, N.G. and Dickinson, J.E. (2014). Fluidized bed desliming in fine particle flotation - Part III Flotation of difficult to clean coal, *Minerals Engineering*, *66-68*, 94-101.

Hadler, K., Smith, C.D., & Cilliers, J.J. (2010). Recovery vs. mass pull: The link to air recovery, *Minerals Engineering*, *23*, 994-1002.

Hapugoda, P., O'Brien, G., Millar, J., Ofori, P., & Firth, B. (2010). Determination of flotation kinetics of coal grain types in a pilot scale jameson cell using coal grain analysis method. In *Proc. XXV International Mineral Processing Congress 2010, IMPC 2010* (pp. 2855-2863). Brisbane, Australia: IMPC.

Harbort, G.J., Cowburn, J.A., & Manlapig, E.V. (2004). Recovery Interactions between the Froth Zone, Pulp Zone and Downcomer within a Jameson cell. In W. Membrey (Ed.), *Proc. 10th Australian Coal Preparation Conference* (pp. 91-101). Pokolbin, Australia: Australian Coal Preparation Society Limited.

Imhof, R., Fletcher, M., Vathavooran, A., & Singh, A. (2007). Application of IMHOFLOT G-Cell centrifugal flotation technology, *Journal of the Southern African Institute of Mining and Metallurgy*, *107*(10), 623-631.

Jameson, G.J. (2009). Advances in fine and coarse particle flotation. In Gomez, C.O. (Ed.), Fundamentals of Mineral Processing, 7th UBC – McGill – UA Biennial International Symposium in Honour of Professor James Finch. Sudbury, Canada.

Jameson, G. (2010). New directions in flotation machine design, *Minerals Engineering*, *23*, 835-841.

Jiang, K., Dickinson, J., & Galvin, K. (2016). Two-stage fast flotation of coal tailings using reflux flotation, *Minerals Engineering*, *98*, 151–160.

Jiang, K., Dickinson, J.E., & Galvin, K.P. (2019). The kinetics of Fast Flotation using the Reflux Flotation Cell, *Chemical Engineering Science*, *196*, 463-477.

Kruglyakov, P.M, Elaneva, S.I., Vilkova, N.G., & Karakashev, S.I. (2010). Investigation of foam drainage using foam pressure drop technique*, Colloids and Surfaces A: Physicochemical and Engineering Aspects*, *354*, 291-297.

Lorenceau, E., Louvet, N., Rouyer, F., & Pitois, O. (2009). Permeability of aqueous foams, *European Physical Journal*, *E28*, 293–304.

Mankosa, M.J., Kohmuench, J.N., Christodoulou, L., & Yan, E.S. (2018). Improving fine particle flotation using the StackCell™ (raising the tail of the elephant curve), *Minerals Engineering*, *121*, 83-89.

Mohanty, M.K., Honaker, B.Q., Patwardhan, A., & Ho, K. (1998). Coal Flotation Washability: An Evaluation of the Traditional Procedures, *International Journal of Coal Preparation and Utilisation*, *19(1-2)*, 33-49.

Neethling, S.J., & Cilliers, J.J. (2001). Simulation of the effect of froth washing on flotation performance, *Chemical Engineering Science*, *56*, 6303–6311.

O'Brien, G., Firth, B., Warren K., & Hapugoda, P. (2013). Improved understanding of coal exploration samples by coal grain analysis, ACARP Project C20040 Final Report, Australian Coal Association.

O'Brien, G., Jenkins, B.M., & Beath, H. (2003). Coal Grain Analysis, ACARP Project C10053 Final Report, Australian Coal Association.

O'Brien, G., Ofori, P., & Jenkins, B. (2007). Semi-automated petrographic assessment of coal by coal grain analysis, *Minerals Engineering*, *20*, 428–434.

Ofori, P.K., O'Brien, G., Firth, B.A., & Jenkins, B. (2006). Flotation process diagnostics and modelling by coal grain analysis, *Minerals Engineering*, *10*, 102–113.

Pratten, S.J., Bensley, C.N., & Nicol, S. (1989). An evaluation of the flotation response of coals, *International Journal of Mineral Processing*, *27*(3-4), 243-262.

Rouyer, F., Pitois, O., Lorenceau, E., & Louvet, N. (2010). Permeability of a bubble assembly: from the very dry to the wet limit, *Physics of Fluids*, *22*, 1–5.

Schulz, N.F. (1970). Separation efficiency, *Trans. Metall. Soc. Am. Inst. Mining, Metall., Petrol. Eng.*, *247* (March), 81–87.

Trahar, W.J., & Warren, L.J. (1976). The flotability of very fine particles – A Review, *Int. J. Miner. Process.*, *3*, 103-131.

Wills, B.A., & Finch, J.A. (2016). *Will's Mineral Processing Technology: An introduction to the practical aspects of ore treatment and mineral recovery* (8th ed.). Oxford, England: Butterworth-Heinemann.

Yianatos, J. B., Finch, J.A., & Laplante, A.R. (1986). Holdup Profile and Bubble Size Distribution of Flotation Column Froths, *Canadian Metallurgical Quarterly*, *25*, 23–29.

Yianatos, J.B., Finch, J.A. & Laplante, A.R. (1987). The cleaning action in column flotation froths, *Trans. of the Institution of Mining and Metallurgy. Section C, Mineral processing and extractive metallurgy*, *96*, C199-C205.

Yianatos, J.B., & Henríquez, F. (2007). Boundary conditions for gas rate and bubble size at the pulp-froth interface in flotation equipment, *Minerals Engineering*, *20*, 625-628.

Yianatos, J.B., Laplante, A.R., & Finch, J.A. (1985). Estimation of local holdup in the bubbling and froth zones of a gas—liquid column, *Chemical Engineering Science*, *40*(10), 1965-1968.

Appendix A: Supplementary Material

Figure A-1 presents the sequential raw head assays for the feed, product and reject for RFC Runs A-G, plotted as a function of the experiment run time.

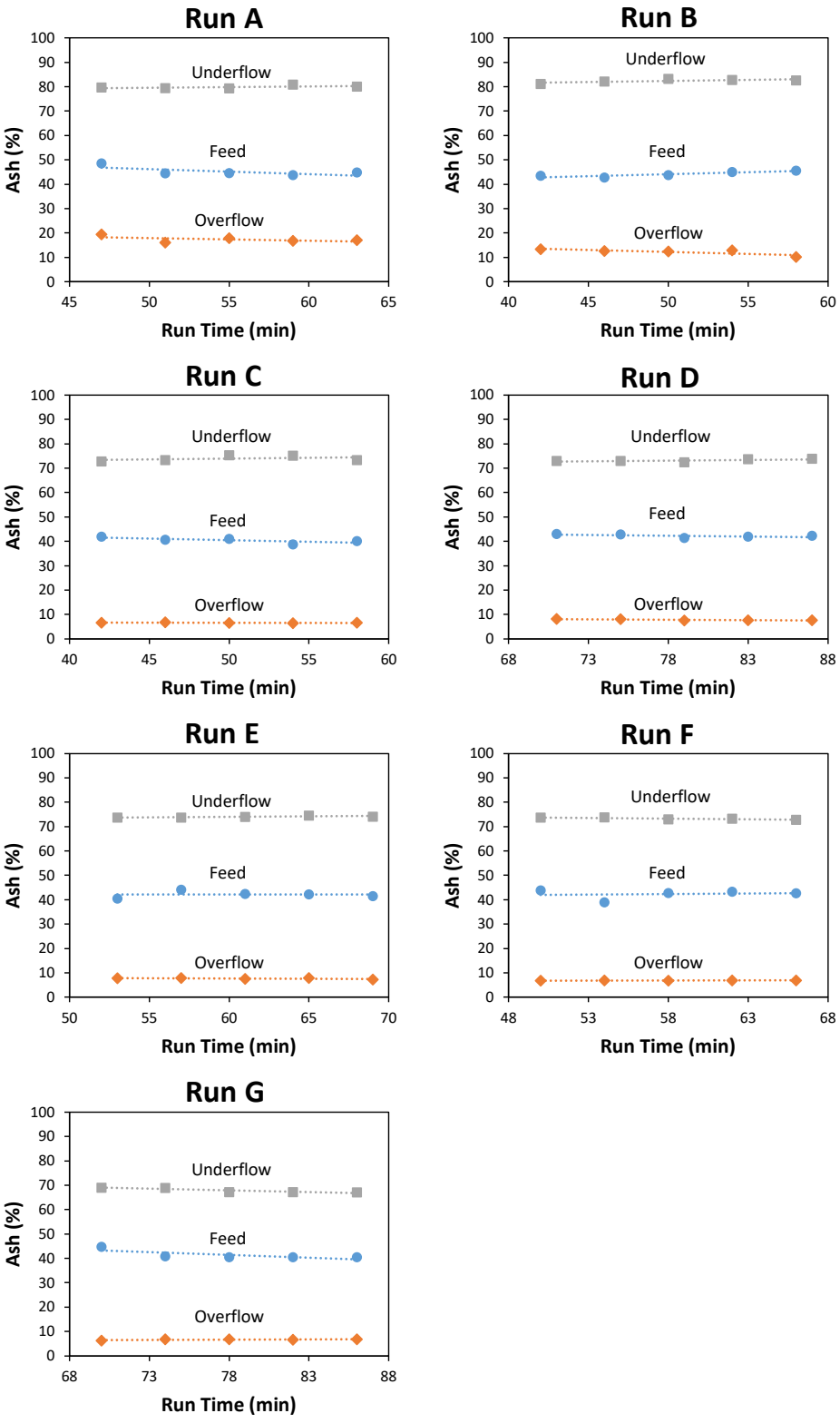

Figure A-1: Sequential raw head ash samples for Runs A - G for feed, overflow and underflow streams, plotted as a function of experiment run time.

Figure A-2 compares the CGA "All grains" recovery-ash curves for both the raw (uncorrected) and corrected data for each of two dosed feed samples collected from the 0.15 m^3 RFC feed tank, and one sample collected prior to reagent addition, sampled from the 2 m^3 conditioning tank. The two dosed feed samples were adjusted to align the final head ash of the feed with that of the average RFC feed ash (42.8% ash), and the sample without any reagent was aligned to the final head ash of the tree flotation results (35.2% ash).

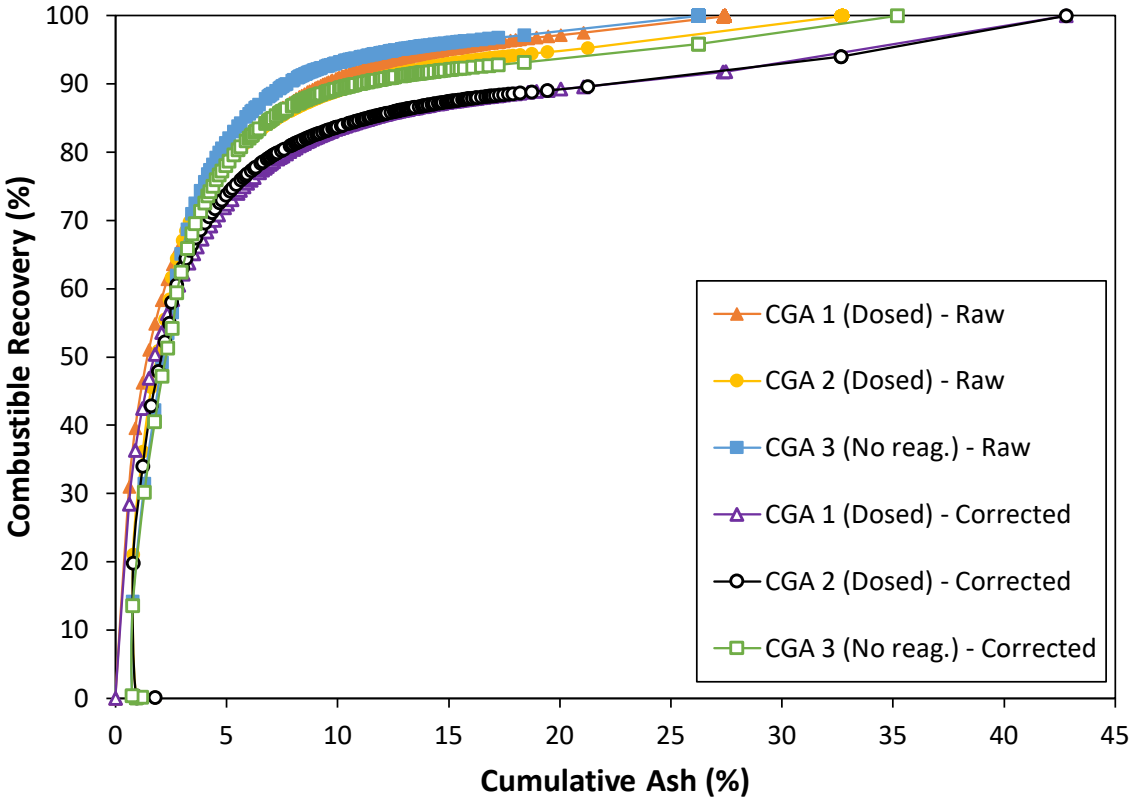

Figure A-2: Comparison of Coal Grain Analysis (CGA) recovery-ash curves generated from the raw data and the corrected data. The corrected CGA curve was adjusted to align the final head ash of the feed with that of the tree flotation results.

Table A-1 below compares the RFC experimental yields of the raw experimental data to that of the mass balanced reconciled data, determined via both the mass flow rate (of the solids reporting to the overflow compared to the feed solids) data and the two-product formula using the ash assay data.

Table A-1: Comparison of yield for each RFC experiment determined via both the raw experimental data and mass balance reconciled data using both the mass flow rates of solids and the ash assays.

	Raw Data Yield (%)		Mass Balanced Yield (%)	
	Mass Flow Rate	**Assay**	**Mass Flow Rate**	**Assay**
Run A	60.4	55.4	58.2	58.1
Run B	49.7	54.6	55.9	55.9
Run C	45.2	49.7	51.1	51.0
Run D	45.3	47.2	47.4	47.4
Run E	42.9	48.1	47.6	47.8
Run F	37.1	46.6	45.9	46.0
Run G	33.7	43.2	38.4	38.5